Electronic Supporting Information

Manganese Oxide-based Mesoporous Thin-Film Electrodes: Manganese Disproportionation Reaction in Alkaline Media**

Irmak Karakaya Durukan[a], Işıl Ulu[a] and Ömer Dag[ab]*

[a.]Department of Chemistry, Bilkent University, 06800, Ankara, Türkiye.
[b.]UNAM — National Nanotechnology Research Center and Institute of Materials Science and Nanotechnology, Bilkent University, 06800, Ankara, Türkiye.

***** Dedicated to Prof. Geoffrey A. Ozin's 80th Birthday***

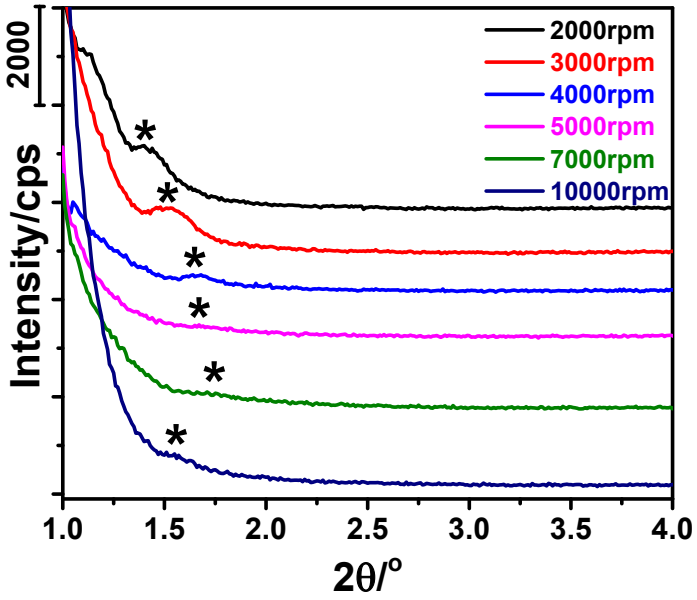

Fig. S1. Small-angle XRD patterns of the $LiNO_3$-$Mn(NO_3)_2$-P123 LLC films after coating of liquid precursor at indicated spin rates.

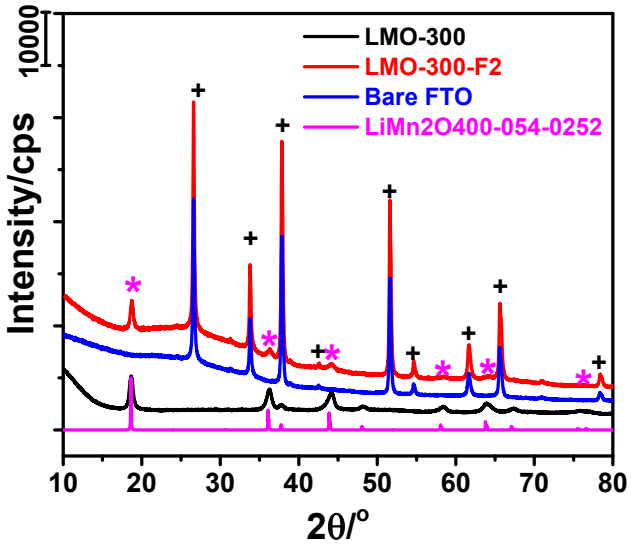

Fig. S2. The wide-angle XRD patterns of the *m*-LMO-300 powder and *m*-LMO-300-F2 film samples. + assigned to SnO_2 using its reference diffraction pattern (ICDD card no. 00-041-1445) and * to $LiMn_2O_4$ lines using the ICDD card no. 00-054-0252.

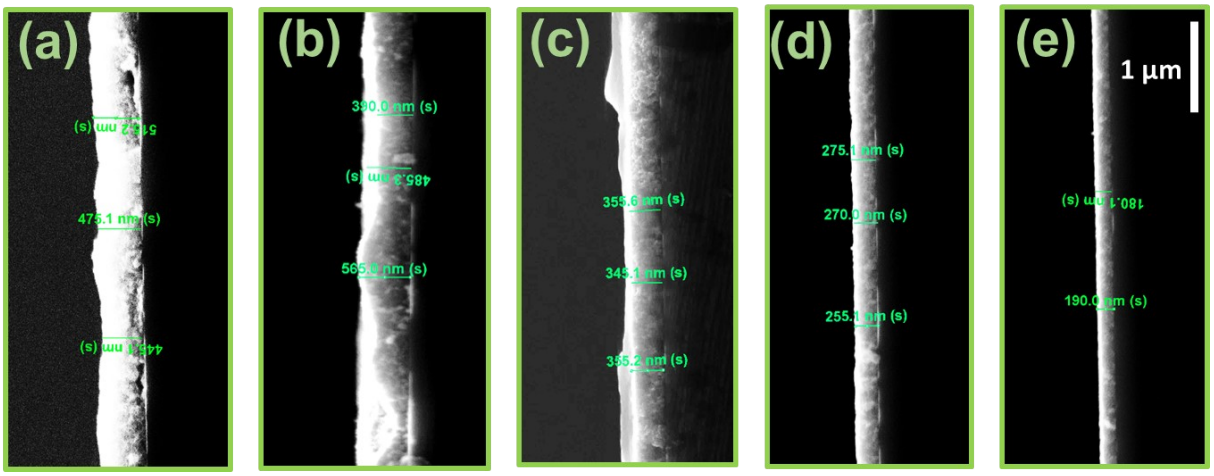

Fig. S3. Cross sectional SEM images of the *m*-LMO thin films, coated at (a) 2000, (b) 3000, (c) 5000, (d) 7000, and (e) 10000 rpm spin rates.

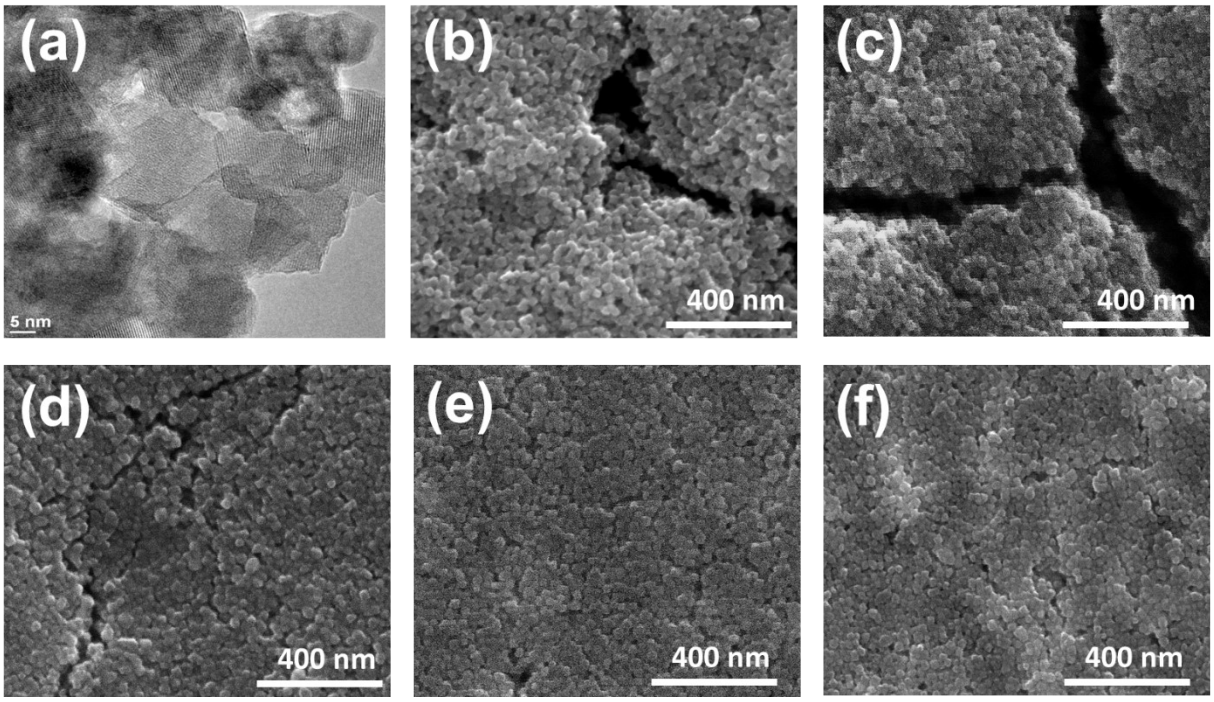

Fig. S4. The TEM (a) and SEM (b) images of the *m*-LMO-300-F2 sample and the SEM images of the *m*-LMO-300-F#, where # is (c) 3000, (d) 5000, (e) 7000, and (f) 10000.

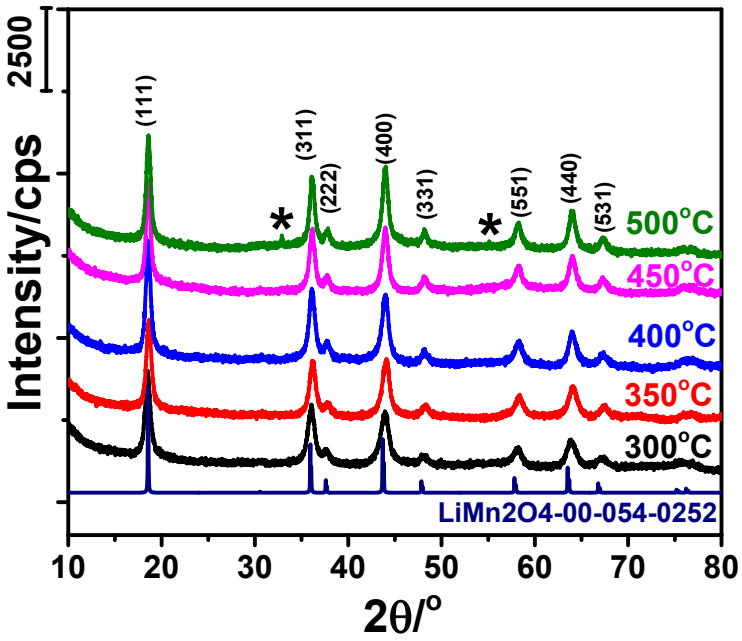

Fig. S5. The powder XRD patterns of the annealed *m*-LMO thick films synthesized by drop casting method, calcined and annealed at indicated temperatures together with the reference pattern of LiMn2O4 from ICDD card no. 00-054-0252. The lines marked * are assigned to Mn_2O_3 using the ICDD card no. 00-041-1442.

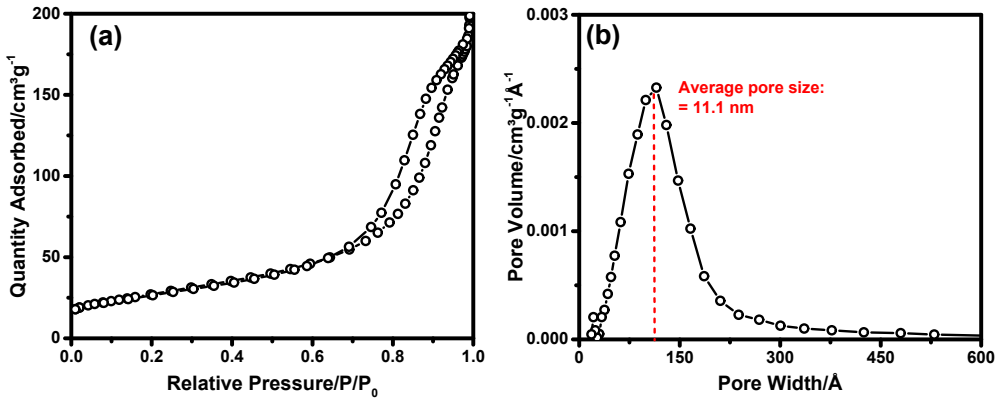

Fig. S6. (a) N_2 (77 K) adsorption-desorption isotherm and (b) BJH pore-size distribution

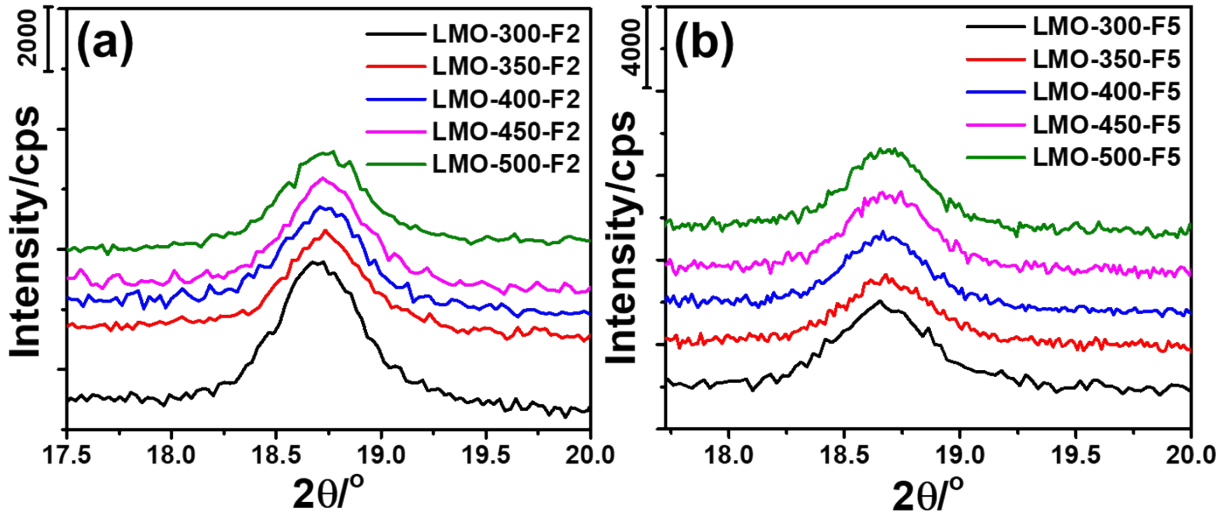

curve of m-LMO-300.

Fig. S7. The XRD patterns between 17.5 and 20.0°, 2θ, of (a) *m*-LMO-X-F2 (b) *m*-LMO-X-F5 (where X is given in the panels).

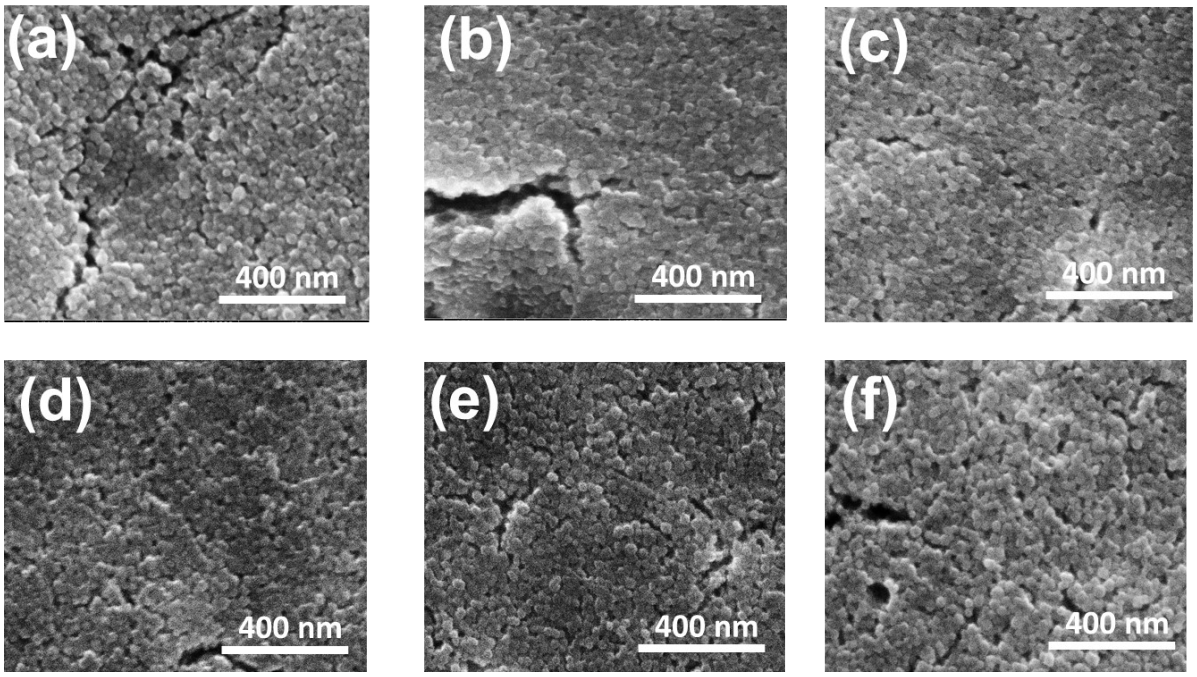

Fig. S8. The SEM images of the *m*-LMO-X-F5 thin films, where X is (a) 300, (b) 350, (c) 400, (d) 450, (e) 500, and (f) 600.

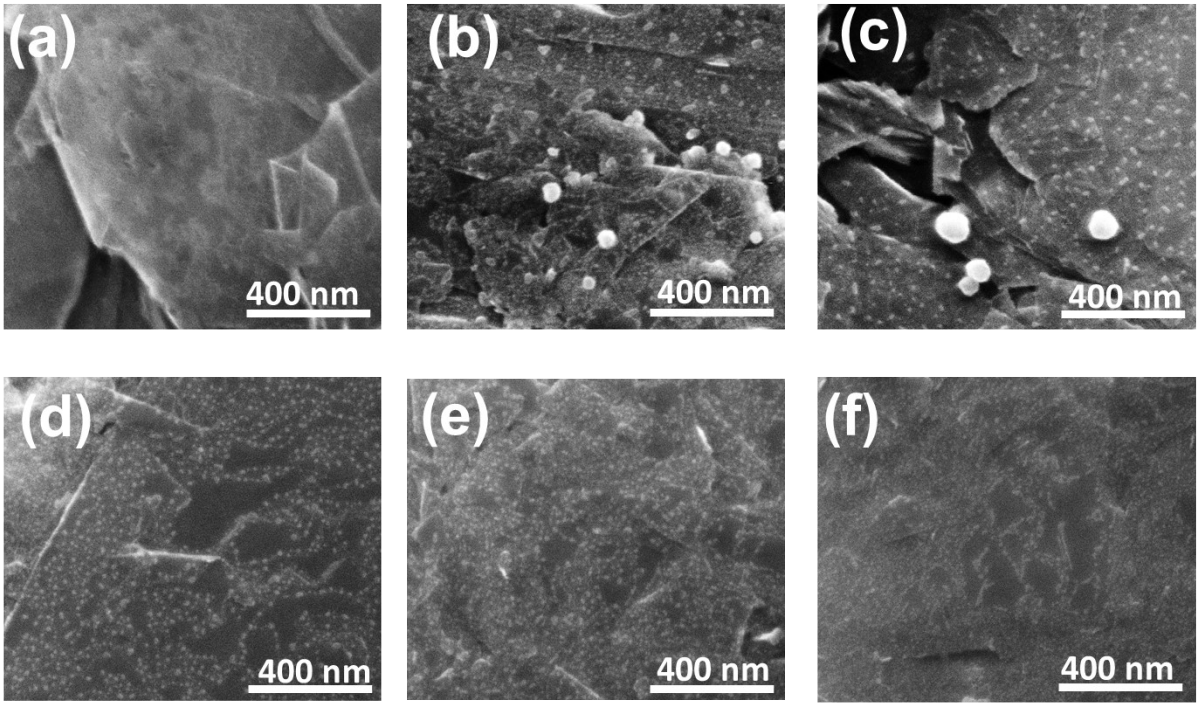

Fig. S9. The SEM images of the (a) bare graphite and *m*-LMO-300-G# thin films, where # is, (b) 5, (c) 10, (d) 20, (e) 50, (f) 100.

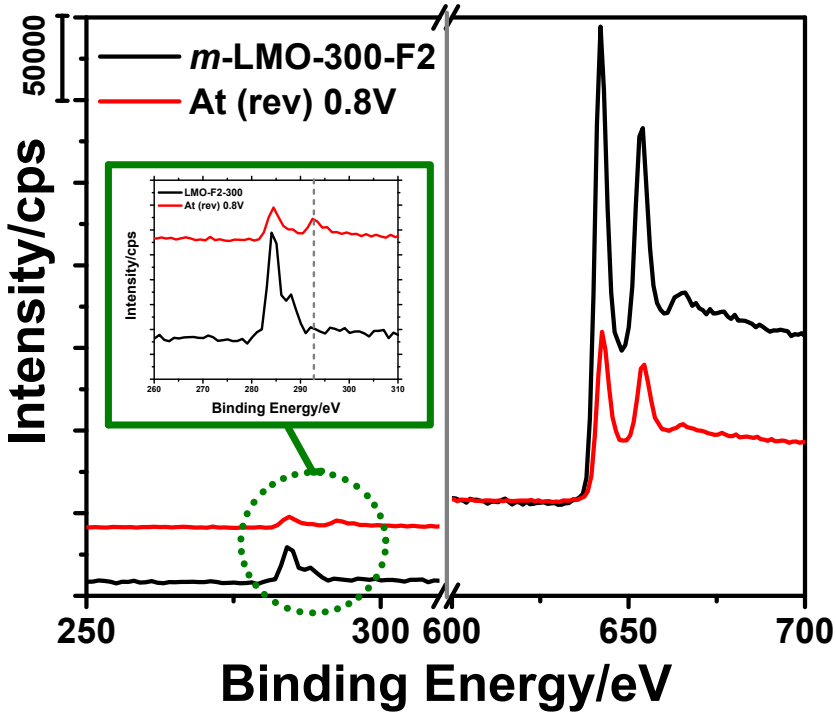

Fig. S10. The XPS survey spectra of the *m*-LMO-300-F2 and *m*-LMO-300-F2 electrodes at (rev) 0.8 V in the 3rd CV curve in 1.0 M KNO_3. Inset graph: magnified XPS spectra of K 2p

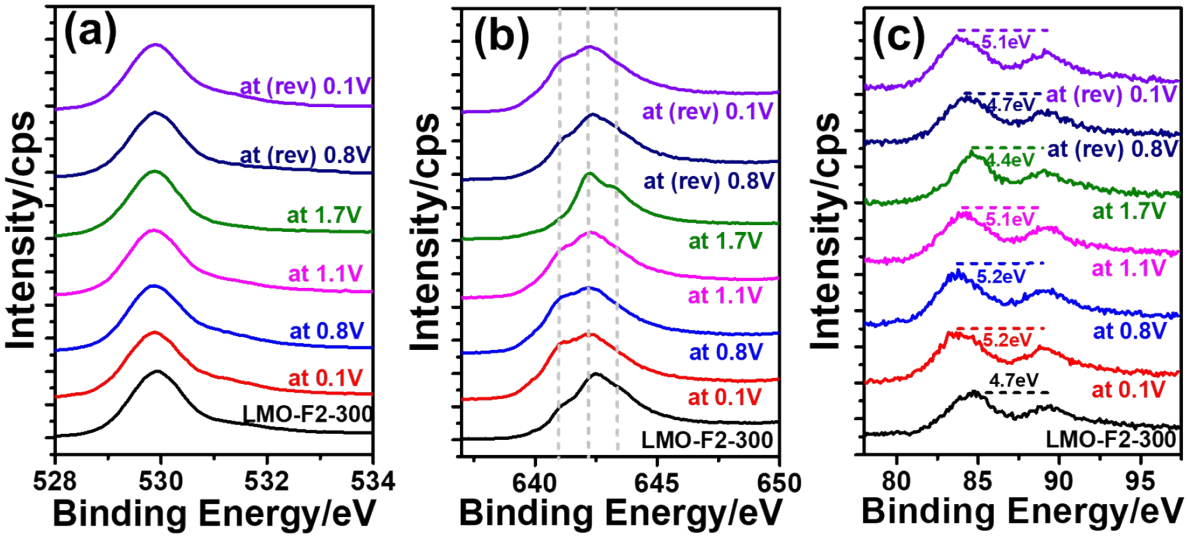

region.

Fig. S11. The XPS spectra of the *m*-LMO-300-F2 electrodes at various potentials (between -0.1 and 1.9 V vs RHE) in 1.0 M $LiNO_3$ in the 1st CV curve in the regions of (a) O 1s, (b) Mn 2p ($^2P_{3/2}$), and (c) Mn 3s.

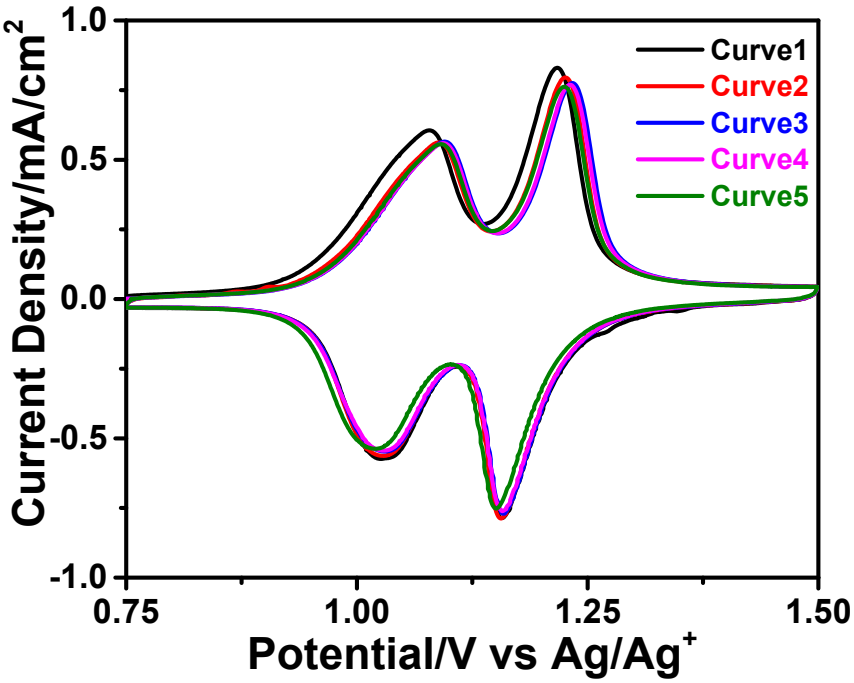

Fig. S12. The CV curves of the *m*-LMO-300-F2 electrode in 1.0 M $LiClO_4$ acetonitrile solution with 5 mV/s in a potential window of 0.75 and 1.5 V vs Ag/Ag^+.

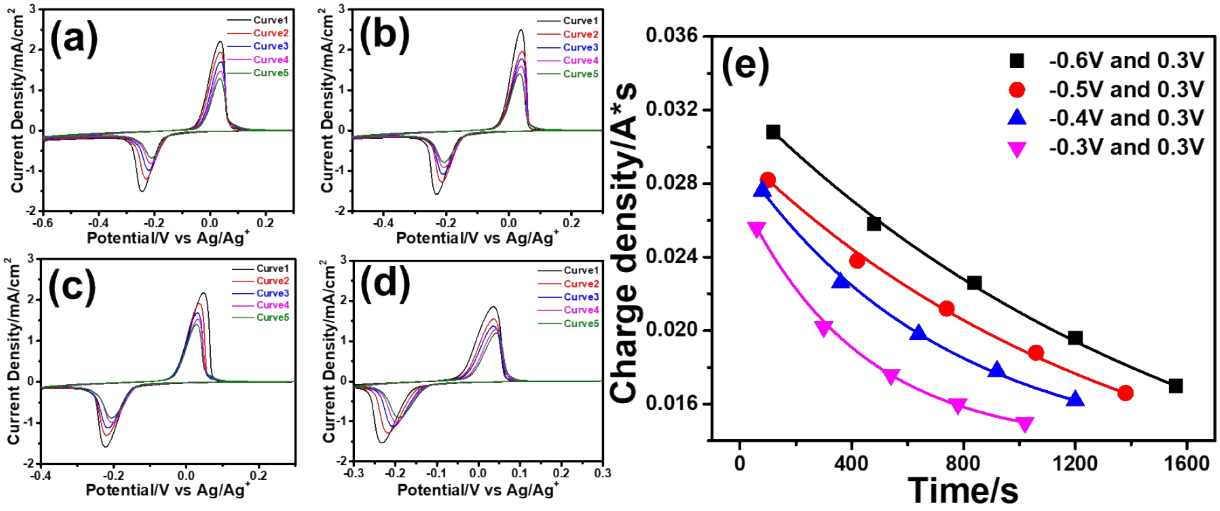

Fig. S13. The CV curves of the *m*-LMO-300-F2 electrode in 1.0 M $LiClO_4$ acetonitrile solution with 5 mV/s scan rate in the potential windows of between x and 0.3 V vs Ag/Ag^+, where x is (a) -0.6, (b) -0.5, (c) -0.4, and (d) -0.3 V. (e) The plot of charge capacity (oxidation peak at 0 V) vs time.

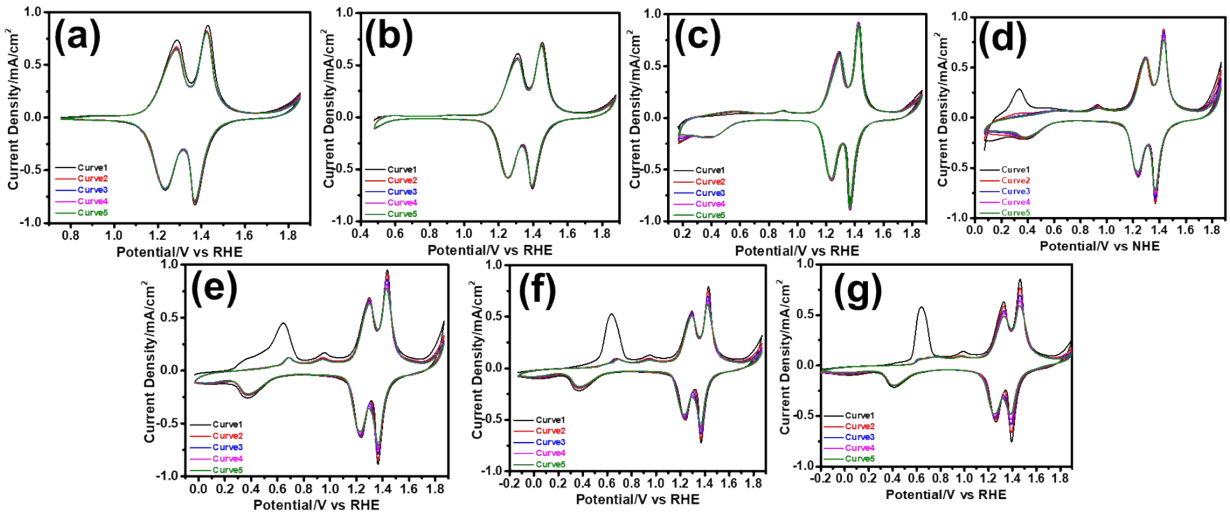

Fig. S14. The CV curves of the *m*-LMO-300-F2 electrode in 1.0 M $LiNO_3$ aqueous solution with 5 mV/s scan rate in potential windows of between x and 1.9 V vs RHE, where x is (a) 0.75, (b) 0.45, (c) 0.15, (d) 0.05, (e) -0.05, (f) -0.15, and (g) -0.2 V.

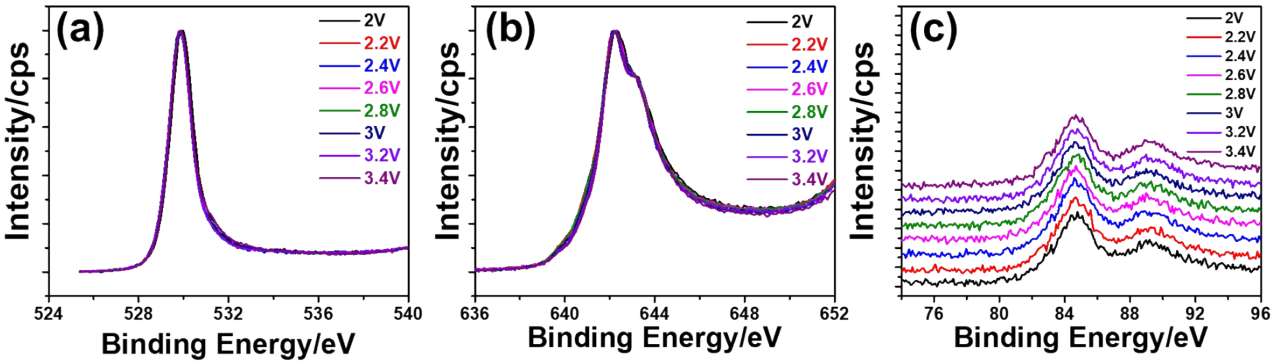

Fig. S15. The XPS spectra of the *m*-LMO-300-F2 electrodes, removed at various potentials in 1.0 M $LiNO_3$, in the regions of (a) O 1s (b), Mn 2p ($^2P_{3/2}$), and (c) Mn 3s.

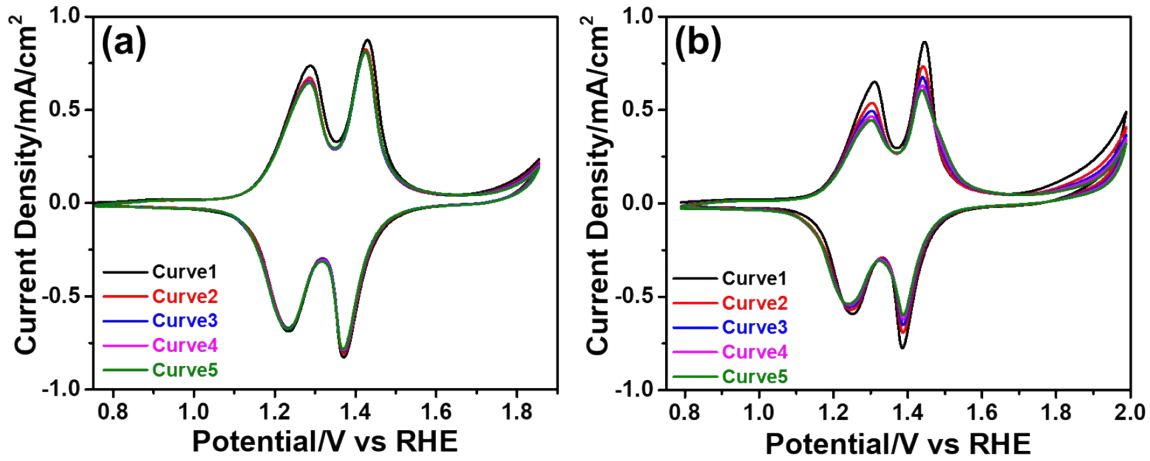

Fig. S16. The CV curves of the *m*-LMO-300-F2 electrode in 1.0 M $LiNO_3$ aqueous solution with 5 mV/s scan rate in the potential windows between 0.75 and xV, where x is (a) 1.9 and (b) 2.0 V.

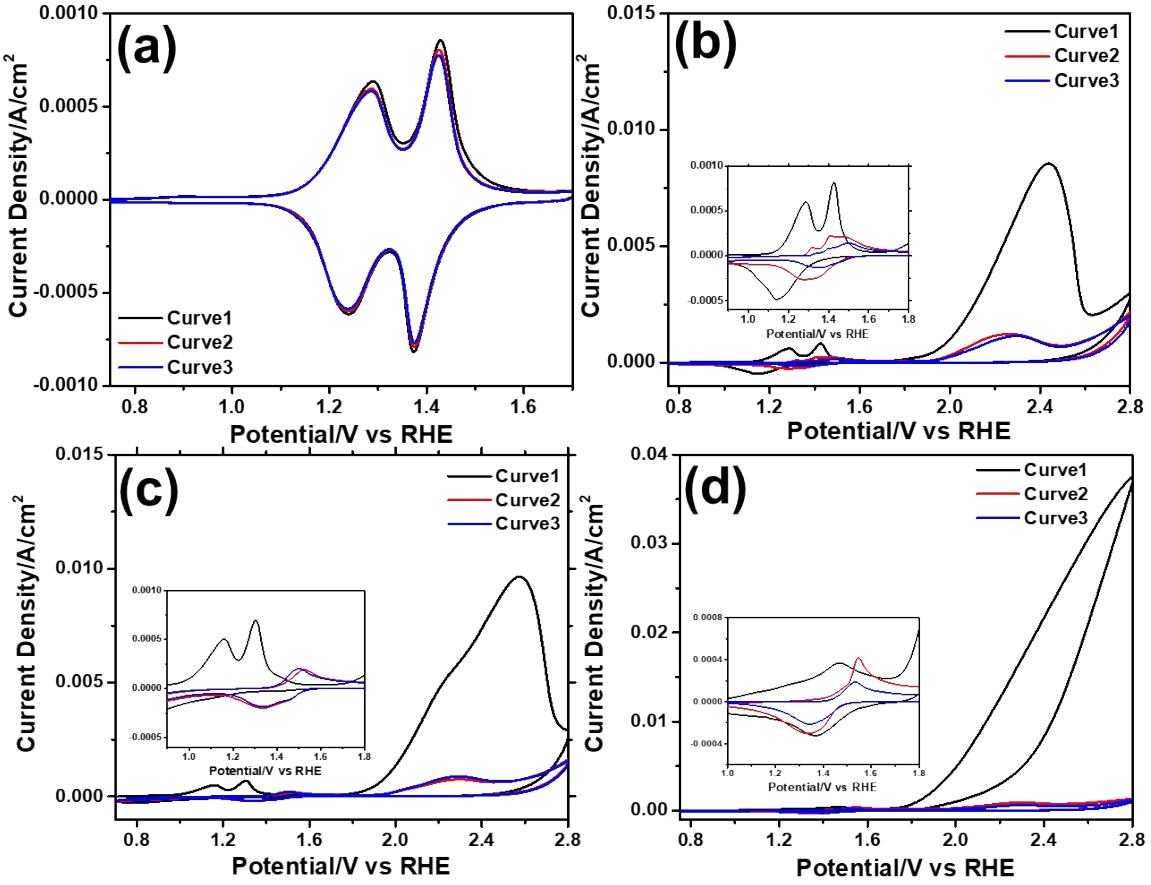

Fig. S17. 3 CV curves the *m*-LMO-300-F2 electrode in 1.0 M $LiNO_3$ aqueous solution with a 5 mV/s scan rate between (a) 0.75 and 1.7 V and (b) between 0.75 and 2.8 V (inset is between 0.9 and 1.8 V), (c) 3 CV curves of the *m*-LMO-300-F2 electrode with 5 mV/s scan rate between 0.75 and 2.8 V (inset is between 0.9 and 1.8 V) in 1.0 M KNO_3 aqueous solution and (d) 3 CV curves of the m-Mn_3O_4-300-F2 electrode between 0.75 and 2.8 V (inset is between 0.9 and 1.8 V) with 5mV/s scan rate in 1.0 M KNO_3 aqueous solution.

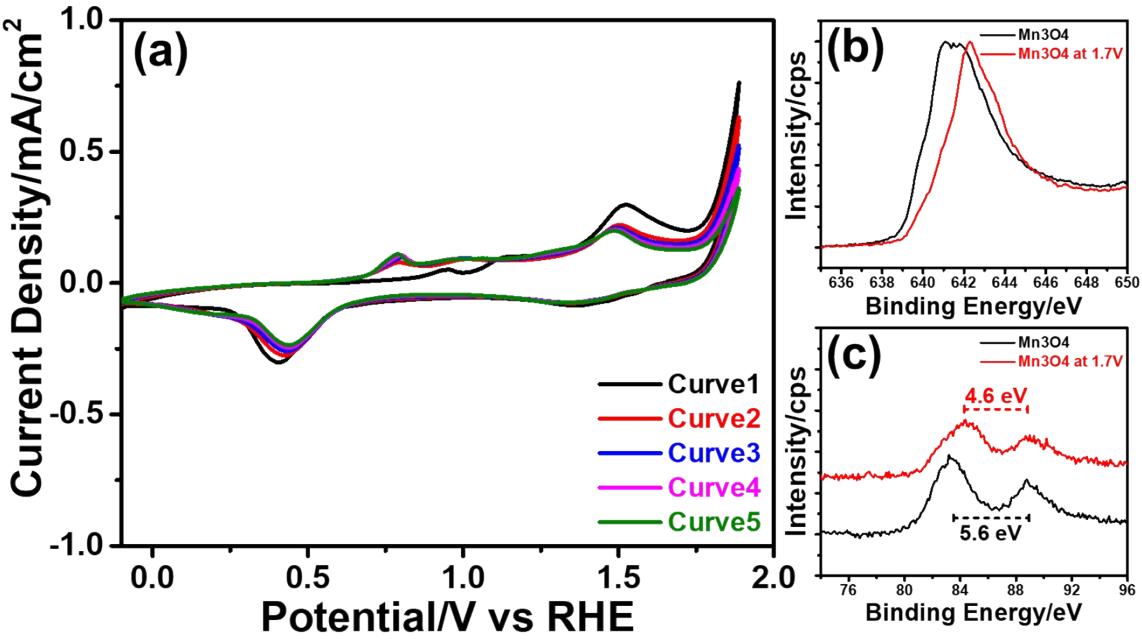

Fig. S18. (a) The CV curves of the *m*-Mn_3O_4-300-F2 electrode with 5 mV/s scan rate in 1.0 M $LiNO_3$ aqueous solution. (b) The XPS spectra of Mn 2p and (c) Mn 3s region of the *m*-Mn_3O_4-300-F2 electrode before and after LSV in 1.0 M $LiNO_3$ aqueous solution between -0.1 and 1.9 V.

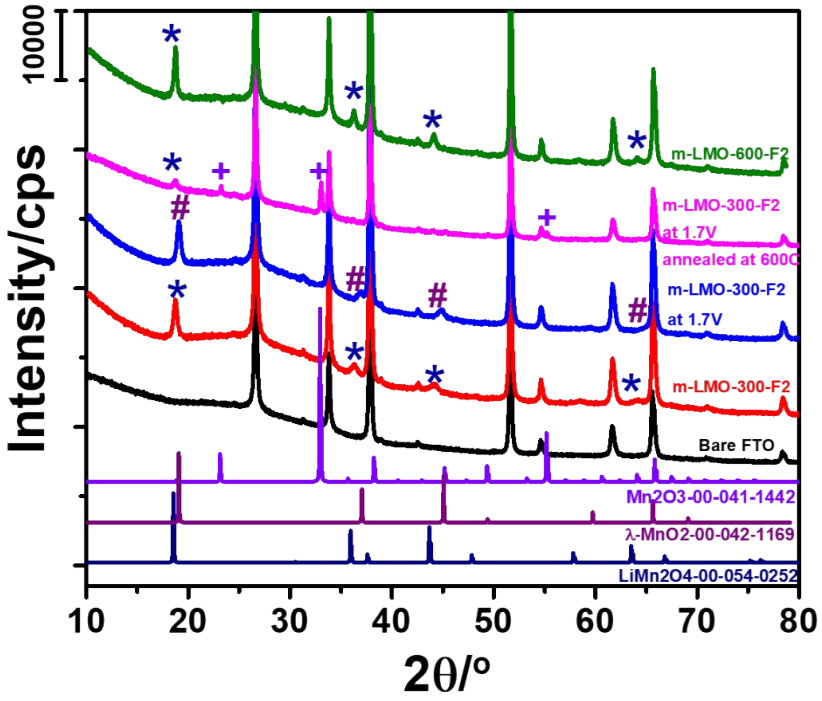

Fig. S19. The XRD patterns of the bared FTO, *m*-LMO-300-F2, *m*-LMO-600-F2, and *m*-LMO-300-F2 annealed at 600 °C after LSV between 0.7 and 1.7 V in 1.0 M $LiNO_3$ aqueous solution and (the XRD patterns of λ-MnO_2, Mn_2O_3, and $LiMn_2O_4$ references from ICDD card no. 00-042-1169, 00-041-1442, and 00-054-0252, respectively).

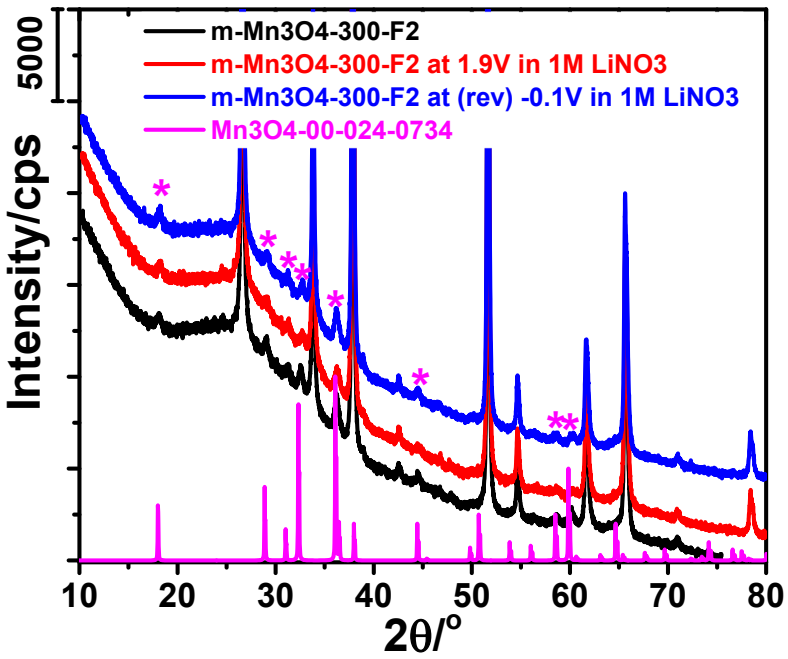

Fig. S20. The XRD patterns of the *m*-Mn_3O_4-300-F2, before and after LSV between -0.1 and 1.9 V and after full cycle between -0.1 and 1.9 V in 1.0 M $LiNO_3$ aqueous solution.

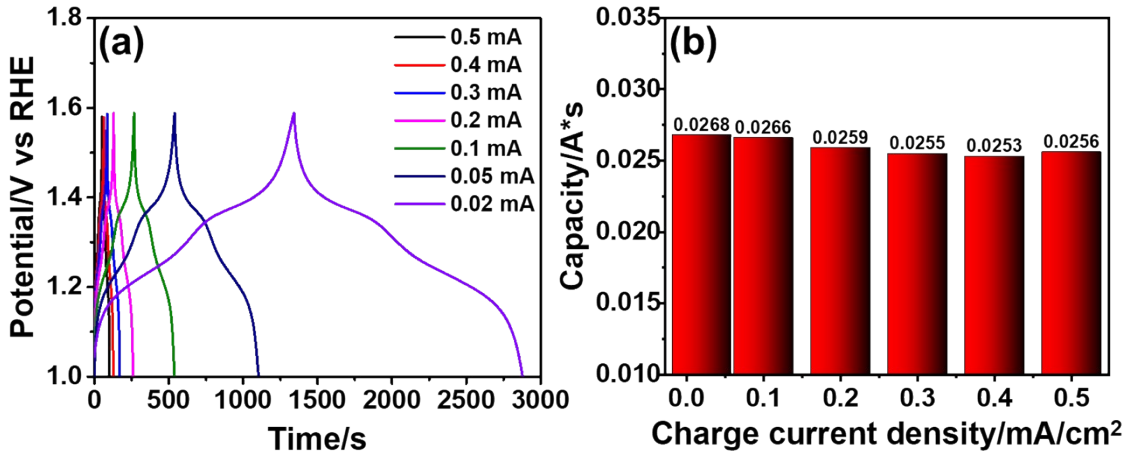

Fig. S21. (a) The GCD curves of the *m*-LMO-300-F2 electrode in 1.0 M $LiNO_3$ at various charge-discharge current densities (indicated in the panel) and (b) charge capacities of the same electrode at various indicated current densities.

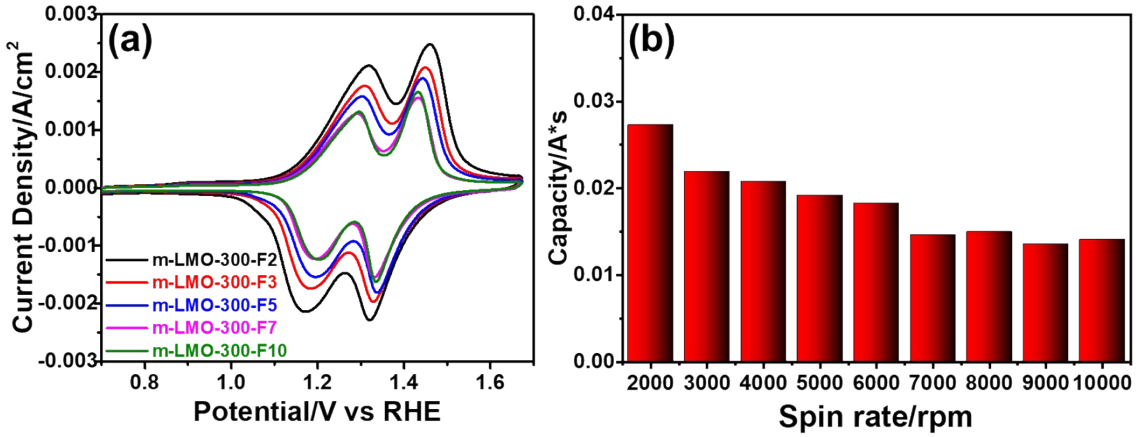

Fig. S22. The CV curves of the *m*-LMO-300-F# (# corresponds to spin rate # thousands) in 1.0 M $LiNO_3$ aqueous solution with a 20 mV/s scan rate and (b) charge capacity vs spin-rate plot of the *m*-LMO-300-F# electrodes.

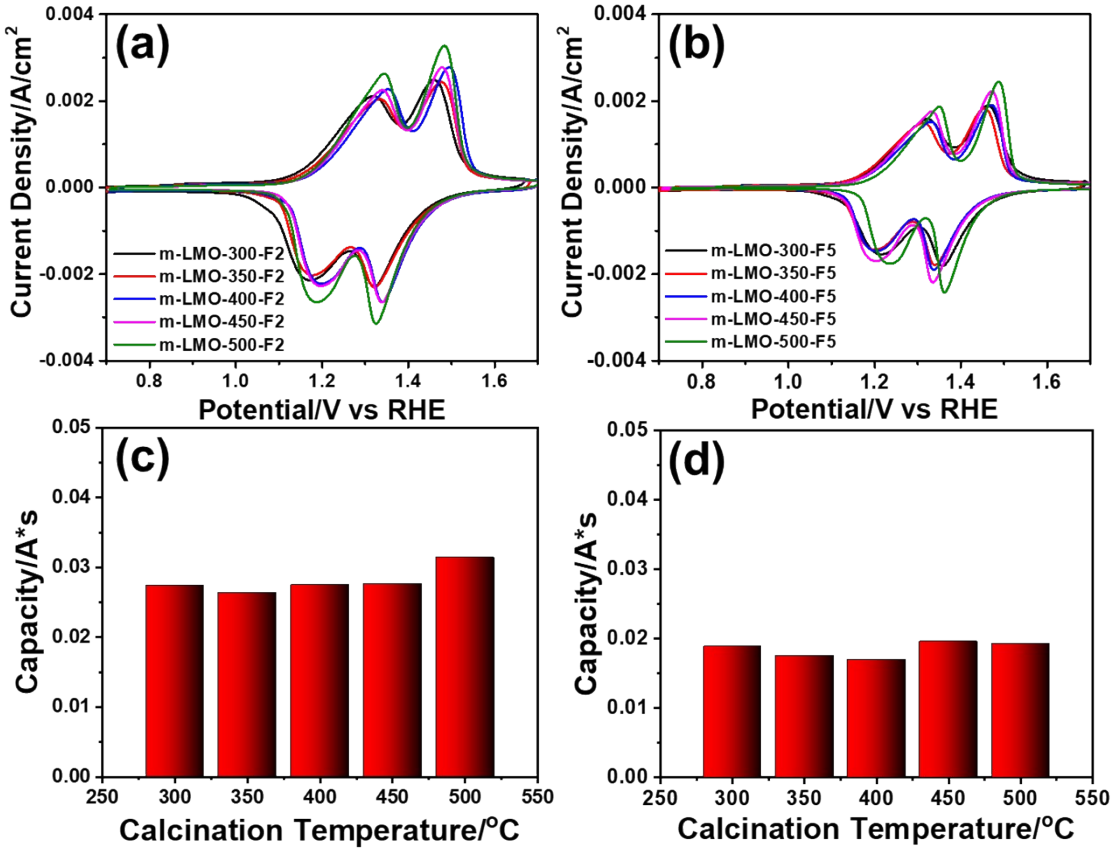

Fig. S23. The CV curves of the *m*-LMO-X-F2 (a), *m*-LMO-X-F5 (b), in 1.0 M $LiNO_3$ aqueous solution with 20 mV/s scan rate, where X is 300, 350, 400, 450, 500. Plot of charge capacity versus calcination/annealing temperature of the (c) *m*-LMO-X-F2, (d) *m*-LMO-X-F5 electrodes.

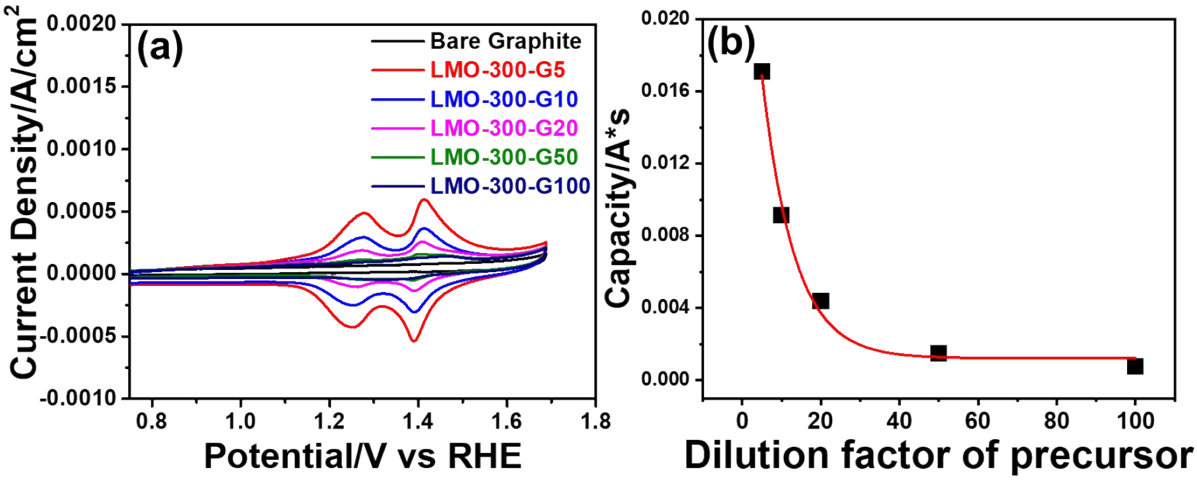

Fig. S24. (a) The CV curves of the *m*-LMO-300-G# electrodes in 1.0 M $LiNO_3$ aqueous solution with 5 mV/s, where # is 5, 10, 20, 50, 100 and (b) the plot of charge capacity versus dilution factor of solution precursor.

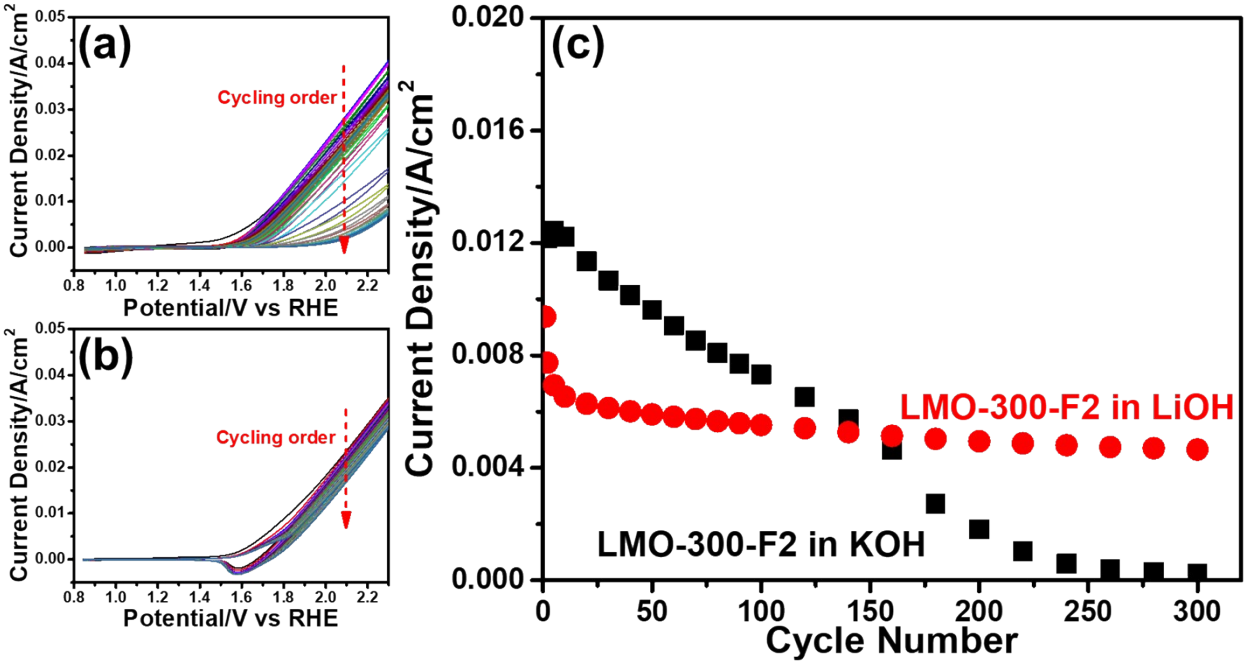

Fig. S25. The CV curves of the *m*-LMO-300-F2 electrode a 50 mV/s scan rate in aqueous solutions of (a) 1.0 M KOH and (b) 1.0 M LiOH. (c) The plots of the current density values at 1.8 V versus cycle number of CV curves in the panels (a) and (b).

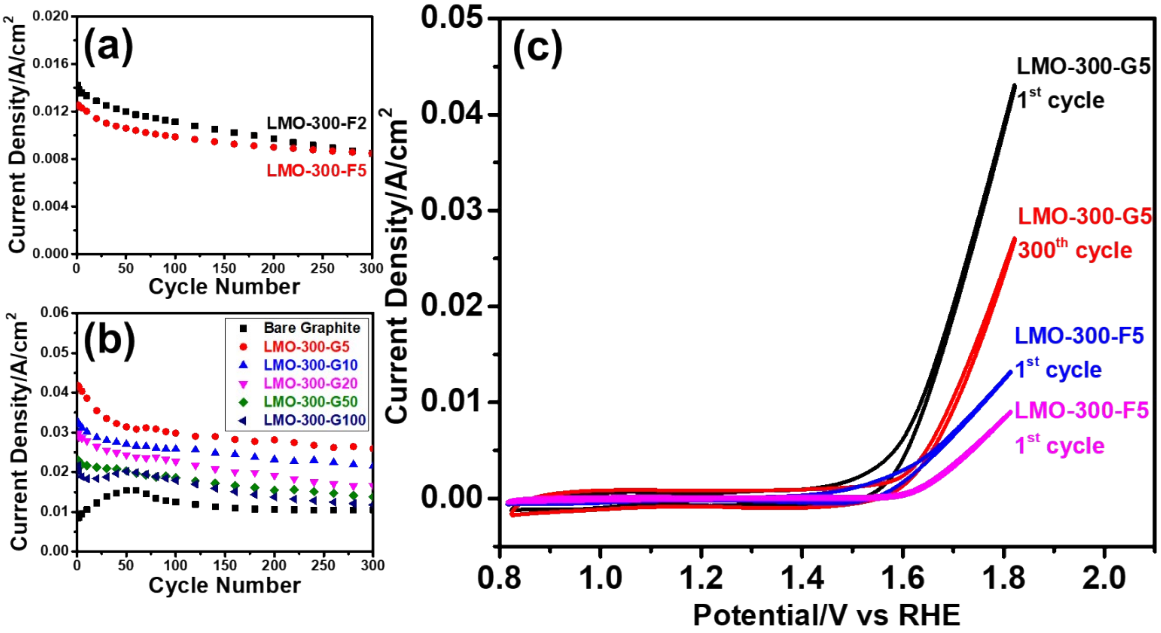

Fig. S26. The plots of the current density values at 1.8 V versus CV (50 mV/s scan rate) cycle number in 1.0 M KOH aqueous solution of the (a) *m*-LMO-300-F2 and *m*-LMO-300-F5 electrodes and (b) *m*-LMO-300-G# electrodes, where # is indicated in the labels. (c) The in the first and 300th CV cycles with a 50 mV/s scan rate in the same electrolytes of the *m*-LMO-300-G5 and *m*-LMO-300-F5 electrodes.

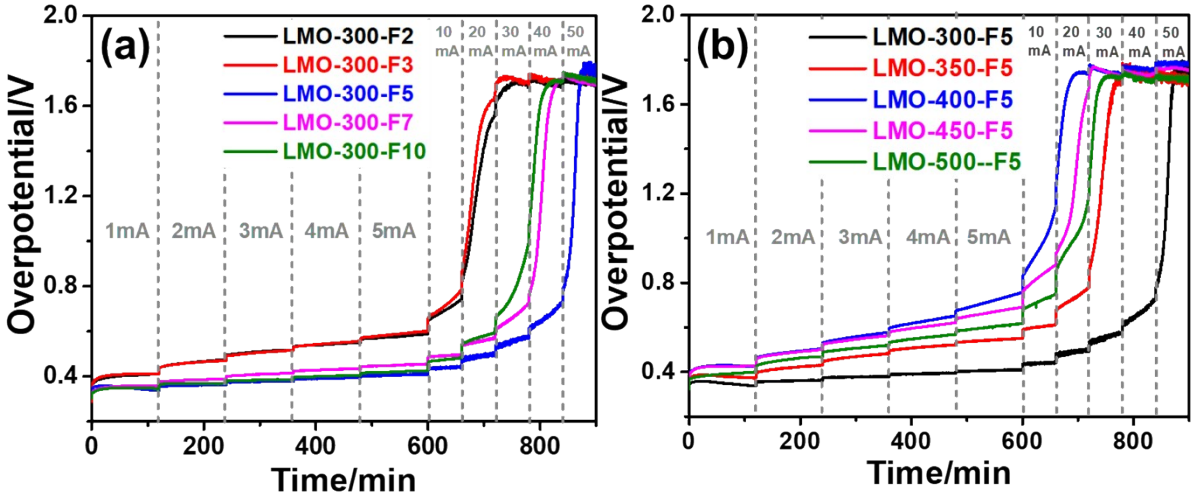

Fig. S27. The multi-step chronopotentiometry plots at various current densities (IR-drop corrected) of the (a) *m*-LMO-300-F# electrodes, where # is 2, 3, 5, 7, and 10 and (b) *m*-LMO-X-F5, where X is 300, 350, 400, 450, and 500.

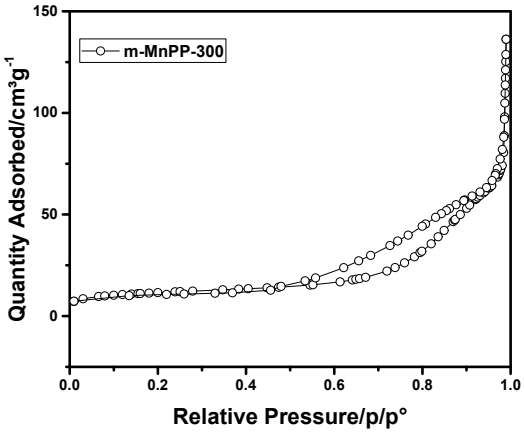

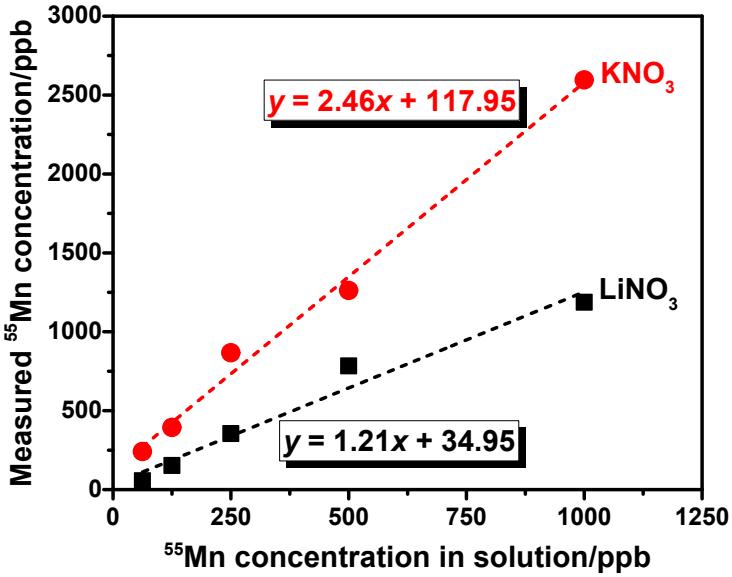

Fig. S28. N_2 (77 K) adsorption-desorption isotherm of m-MnPP-300.

Fig. S29. ICP-MS calibration curves, recorded in acidified 1M KNO_3 and 1M $LiNO_3$ solutions.

Table S1. The charge capacities and catalytic loads of the *m*-LMO-300-F# electrodes.

Electrode	Capacity /A*s	Catalytic load on FTO/μg/cm^2
m-LMO-300-F2	0.0273	61.1
m-LMO-300-F3	0.0219	49.1
m-LMO-300-F4	0.0208	46.5
m-LMO-300-F5	0.0192	42.9
m-LMO-300-F6	0.0183	40.9
m-LMO-300-F7	0.0146	32.7
m-LMO-300-F8	0.0150	33.5
m-LMO-300-F9	0.0136	30.4
m-LMO-300-F10	0.0141	31.5

Table S2. The charge capacities and catalytic loads of the *m*-LMO-X-F2 and *m*-LMO-X-F5 electrodes, where X is 300, 350, 400, 450, 500.

Electrode	Capacity /A*s	Catalytic load on FTO/μg/cm^2
m-LMO-300-F2	0.0273	61.1
m-LMO-350-F2	0.0264	59.1
m-LMO-400-F2	0.0275	61.6
m-LMO-450-F2	0.0276	61.8
m-LMO-500-F2	0.0214	70.3
m-LMO-300-F5	0.0189	42.3
m-LMO-350-F5	0.0176	39.4
m-LMO-400-F5	0.0170	38.1
m-LMO-450-F5	0.0196	43.8
m-LMO-500-F5	0.0193	43.2

Table S3. The charge capacities and catalytic loads of the *m*-LMO-300-G# electrodes, where # is 5, 10, 20, 50, 100.

Electrode	Capacity /A*s	Catalytic load on FTO/μg/cm^2
m-LMO-300-G5	0.0171	38.3
m-LMO-300-G10	0.0092	20.6
m-LMO-300-G20	0.0044	9.9
m-LMO-300-G50	0.0015	3.3
m-LMO-300-G100	0.0007	1.5

Calatalytic load calculation from CV measurements.

$$oad\ (\mu g/cm^2) = \frac{q\left(\frac{A\cdot s}{cm^2}\right)\times 180.8\left(\frac{g}{mol}\right)\times 10^6\left(\frac{\mu g}{g}\right)\times 100}{\left(\frac{A\cdot s}{e}\right)} \quad (Equation\ S1)$$

Where, q is the calculated charge density ($A\cdot s\cdot cm^{-2}$) and 180.8 $g\cdot mol^{-1}$ is the molecular mass of $LiMn_2O_4$.

ICP-MS Calibration Curves

Fig. S29 shows the calibration curves using Mn standard solutions similar to the electrolyte solutions used in this investigation. The calibration curves show that potassium ions (by forming $^{39}K^{16}O^+$) interfere with manganese. Manganese concentrations were determined to be higher than actual values (about 2.46 times higher in KNO_3 and 1.21 time in $LiNO_3$ solutions). The corrected manganese in KNO_3 and $LiNO_3$ electrolytes are tabulated in Table S4.

Table S4. Corrected Mn concentrations in in KNO_3 and $LiNO_3$ electrolytes (S1: m-Mn_3O_4 in KNO_3 0.75 to 2.8V, S2: m-LMO in KNO_3 0.75 to 2.8V, S3: m-LMO in $LiNO_3$ 0.75 to 2.8V, S4: m-LMO in $LiNO_3$ 0.75 and 1.7V, and S5: m-LMO in $LiNO_3$ -0.15 and 1.9V).

Solutions	Experimental ppb	Corrected Mn	Mn Amount (µg) in 20 ml of electrolyte	Degredation % in $LiMn_2O_4$
S1	4635	1836	41.96	-
S2	2738	1065	24.34	65
S3	1163	932	21.30	57
S4	76	34	0.77	2
S5	562	435	9.94	26